

Sensitivity Comparison of Mx and Frequency-Modulated Bell–Bloom Cs Magnetometers in a Microfabricated Cell

Ricardo Jiménez-Martínez, W. Clark Griffith, Ying-Ju Wang, Svenja Knappe, John Kitching, Ken Smith, and Mark D. Prouty, *Member, IEEE*

Abstract—We compare the sensitivity performance of two optically pumped atomic magnetometers based on the Mx and frequency-modulated Bell–Bloom configurations. The Cs magnetometers are implemented using a millimeter-scale microfabricated vapor cell. It is found that the Bell–Bloom magnetometer yields sensitivities similar to those of the Mx magnetometer when operated under equally optimized conditions. The Bell–Bloom approach offers several attractive features over the Mx approach for chip-scale magnetometer instrumentation.

Index Terms—Chip-scale atomic magnetometer, frequency-modulated (FM) light, microfabricated vapor cell, optically pumped atomic magnetometer, vertical-cavity surface-emitting laser (VCSEL).

I. INTRODUCTION

AMONG THE different techniques used to measure magnetic fields [1], the optically pumped atomic magnetometer has recently experienced considerable attention [2]. Magnetometer sensitivities in the subfemtotesla range have been achieved [3], and the development of highly miniaturized microfabricated magnetometers [4] has enhanced the possibility of widespread use in real-world applications that require simple low-cost instrumentation. Atomic magnetometers can be used in a variety of important applications including magnetocardiography [5]–[7], magnetoencephalography [8], detection of nuclear magnetic resonance (NMR) [9], [10], nuclear quadrupole resonance [11], magnetic particle detection [12], and geophysical mapping [13]. Highly miniaturized microfabricated atomic magnetometers offer the advantages of portability,

versatility, low power consumption, and low cost of operation and production while maintaining sensitivities far better than other magnetic sensor technologies with comparable size and power requirements.

For the measurement of magnetic fields in the low geomagnetic range (0.1–20 μT), the most sensitive chip-scale atomic magnetometer [14] implemented so far uses the Mx technique [15]. This Mx magnetometer achieves sensitivities of 5 pT/ $\sqrt{\text{Hz}}$ in an ambient field of 5.5 μT with a sensor head that occupies a volume of 12 mm³ and nominally consumes 194 mW of power [15]. Although the chip-scale Mx magnetometer represents a very appealing magnetic-sensing solution where larger Mx atomic magnetometers are already in use, it is not the best alternative for every application. The RF coils inherent to the Mx magnetometer represent a serious drawback for some applications. In array-based magnetometers, the RF coils can be a source of systematic errors due to the crosstalk among the magnetometers in the array. The misalignment of the RF coil's axis relative to the pumping beam is also a source of systematic errors in the form of spurious phase shifts, as pointed out in [16]. In miniaturized magnetometers, with magnetic resonance linewidths on the order of a few kilohertz, a misalignment between the RF coil's axis and the pumping beam of 1° is reflected as an apparent magnetic change of $>\sim 10$ nT. Furthermore, the Mx magnetometer has two dead zones (an equatorial zone when the pumping light is perpendicular to the magnetic field and a polar zone when the pumping light is parallel to the magnetic field).

In an attempt to mitigate these problems and to produce a simpler magnetometer design that operates in the low geomagnetic range, we have investigated the performance of the Bell–Bloom (BB) magnetometer [17] with FM light in a microfabricated vapor cell. The BB magnetometer is advantageous because the Larmor precession is optically driven and therefore does not suffer from the problems associated with RF coils, it only has one dead zone (a polar one), and it can be realized in some forms with no electrical connections to the sensor head.

The original proposal of an atomic magnetometer with modulated light dates back to 1961 [17]. Since then, extensive work on atomic magnetometers with modulated light has been carried out [18]–[26]. In our approach, we use a vertical-cavity surface-emitting laser (VCSEL) as the source for optical pumping and probing and modulate its injection current to generate the FM

Manuscript received October 6, 2008; revised February 11, 2009. First published September 18, 2009; current version published January 7, 2010. This work was supported by the Strategic Environmental Research and Development Program. The work of R. Jiménez-Martínez was supported by the Roberto Rocca Education Program. The Associate Editor coordinating the review process for this paper was Dr. Juha Kostamovaara.

R. Jiménez-Martínez is with the Department of Physics, University of Colorado at Boulder, Boulder, CO 80309 USA (e-mail: jimenezm@colorado.edu; Ricardo.Jimenezmartinez@colorado.edu).

W. C. Griffith, S. Knappe, and J. Kitching are with the Time and Frequency Division, National Institute of Standards and Technology, Boulder, CO 80305 USA.

Y.-J. Wang is with Cymer, Inc., San Diego, CA 92127 USA.

K. Smith and M. D. Prouty are with Geometrics, Inc., San Jose, CA 95131 USA.

Color versions of one or more of the figures in this paper are available online at <http://ieeexplore.ieee.org>.

Digital Object Identifier 10.1109/TIM.2009.2023829

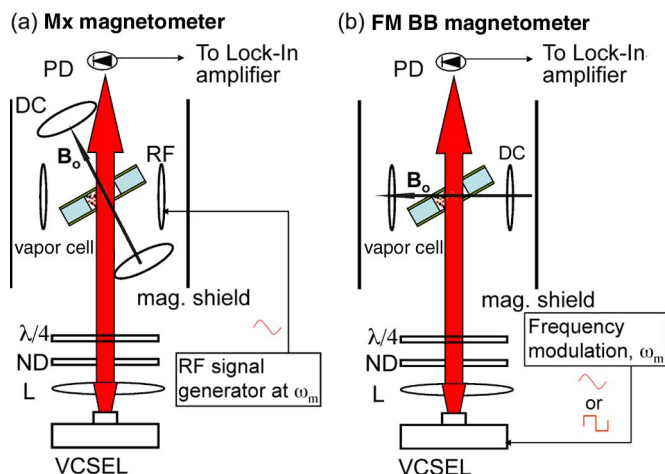


Fig. 1. Experimental setup used in (a) Mx and (b) FM BB magnetometers. L—lens; ND—neutral-density filter; $\lambda/4$ —quarter-wave plate; RF—RF coils; DC—Helmholtz coils to generate dc magnetic field (B_0); PD—photodetector and transimpedance amplifier.

light; we use Cs as the resonant atomic vapor and high pressures of N_2 buffer gas confined in a microfabricated cell. The modulation of the VCSEL current modulates the laser frequency and its amplitude. For the modulation depth of the VCSEL current used in this paper, the effects of FM in optical pumping overwhelm those of AM. To achieve equivalent modulation of the optical pumping rate using AM, the light would have to be more or less completely attenuated by switching the laser current on and off or by using additional modulating devices [18]–[20]. In terms of device manufacturing, our approach is advantageous because it uses fewer components, is amenable for miniaturization, and has the potential for wafer-level fabrication and assembly [14], [15].

In this paper, we demonstrate that the FM BB magnetometer, implemented in a microfabricated miniature vapor cell, can yield sensitivities equivalent to those of the Mx magnetometer. For different atomic densities, we optimize the Mx magnetometer by choosing the RF and optical power that yields the best attainable sensitivities. Similarly, we study how parameters such as the FM waveform, the FM amplitude, and the waveform duty cycle affect the sensitivity of the BB magnetometer. We select the optimum values of these parameters and observe an FM BB magnetometer whose performance is similar to that obtained in the optimized Mx magnetometer.

II. EXPERIMENTAL SETUP

In this paper, the FM BB magnetometer and the Mx magnetometer [27] are implemented using the same vapor cell and the same generic setup. The essential components in the setup are shown in Fig. 1.

The heart of most atomic magnetometers is the vapor cell, which contains the alkali atoms that probe the magnetic field to be measured. In our setup, we use a miniature microfabricated vapor cell constructed as in [28]. The microfabricated vapor cell is constructed by etching a $2\text{ mm} \times 1\text{ mm}$ hole in a 1-mm-thick silicon wafer. Two thin glass wafers are anodically bonded on the top and bottom surfaces of the silicon wafer to her-

metically seal the $2\text{ mm} \times 1\text{ mm} \times 1\text{ mm}$ cavity. Before the second glass wafer is bonded, the cavity is filled with ^{133}Cs and 133 kPa of N_2 buffer gas to avoid the fast depolarization rate of the ^{133}Cs atoms caused by collisions with the cell walls. Another way to reduce surface relaxation is to use surface coatings [2], [19] such as paraffin. However, to date, the most effective and widely used coating, i.e., paraffin, does not withstand the high temperatures (above $300\text{ }^\circ\text{C}$) required in the production process of our microfabricated vapor cells [28].

The 133-kPa N_2 buffer gas pressure broadens the ^{133}Cs optical absorption line to ~ 20 -GHz full-width at half-maximum [see Fig. 3(a)]. Because of this large broadening, neither a ground-state nor an excited-state hyperfine structure can be resolved in the optical absorption spectrum. The cell is heated by sandwiching it between two transparent resistive indium–tin–oxide (ITO) heaters. The ITO heaters are operated in such a way that the magnetic field produced by the current flowing through one of them largely cancels the magnetic field produced by the current flowing through the other [15]. For the measurements reported here, we operated the vapor cell at different atomic densities to change the optical depth of the vapor. The magnitude of the current flowing through the heaters is adjusted until the desired optical depth is reached. The optical depth is defined as $OD = \sigma'nl$, where σ' corresponds to the pressure-broadened resonant absorption cross section of ^{133}Cs , n is the atomic density, and $l \approx 1\text{ mm}$ corresponds to the length of the cell along the light propagation axes. We did not directly measure the temperature; however, from absorption measurements, we can estimate the ^{133}Cs density. For instance, the lowest ($OD = 0.13$) and largest ($OD = 1.35$) values of optical depth used in the experiment correspond to atomic densities of 3.7×10^{12} and $3.8 \times 10^{13}\text{ cm}^{-3}$, respectively, which, in turn, correspond to temperatures of $\sim 80\text{ }^\circ\text{C}$ and $\sim 116\text{ }^\circ\text{C}$, respectively.

The ^{133}Cs atoms are pumped and probed with a single circularly polarized laser beam emitted by a VCSEL. The VCSEL generates 1 mW of optical power at an operating current of 3.5 mA at $72.3\text{ }^\circ\text{C}$. Due to losses in the laser-beam path, the maximum optical power available at the cell is about $200\text{ }\mu\text{W}$. The VCSEL frequency is tuned to the ^{133}Cs $D1$ line (894.6 nm) by controlling the laser temperature. The injection current was operated in an open-loop configuration; the frequency drift of the laser is below 1 GHz over a period of 1 h. The VCSEL light is collimated and passed through a neutral density filter to attenuate the beam power and a quarter-wave plate to make the light polarization circular before the beam is sent to the vapor cell. The beam's cross-sectional profile filled the cell window, giving a beam diameter of $\sim 2\text{ mm}$. To avoid etalon fringes created by the cell surfaces, the vapor cell is tilted by $\sim 45^\circ$ with respect to the laser-beam direction.

The vapor cell is shielded from laboratory magnetic fields by placing it inside a cylinder of material with high magnetic permeability. The shield is equipped with two sets of Helmholtz coils to provide the static magnetic field to be measured and the RF field in the Mx magnetometer. The transmitted light is collected using a photodetector and amplified with a transimpedance amplifier. The signal is demodulated using a lock-in amplifier with a reference frequency equal to the Larmor

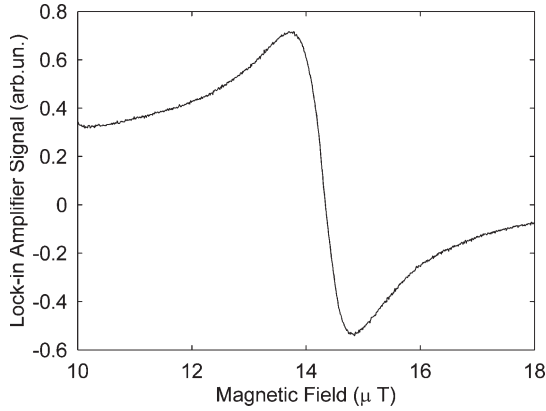


Fig. 2. Dispersive signal as a function of magnetic field. The frequency of the applied RF field is 50 kHz.

frequency. The magnetic resonance signals and their noise are measured as indicated in the following section.

III. MX MAGNETOMETER

In both Mx and FM BB magnetometers, the light from the VCSEL is used both to optically pump the atoms and to monitor their precession about the magnetic field to be measured. The VCSEL frequency is tuned to the center of the pressure-broadened ^{133}Cs $D1$ absorption line by measuring the absorption of the light as a function of frequency. The magnetic field to be measured ($B_o = 14.285 \mu\text{T}$) is provided by a set of Helmholtz coils whose axis is oriented 45° with respect to the optical beam. Free-induction decay measurements were used to calibrate B_o . A second set of Helmholtz coils produces the RF field to coherently drive the precession of the atomic spin about the static magnetic field, at the Larmor frequency (50 kHz). The ^{133}Cs atomic spin precession modulates the transmitted light intensity, which is collected by a photodetector. The photodetector signal is then sent to the lock-in amplifier, which demodulates it at 50 kHz. The light power and the RF coils' current are adjusted to optimize the sensitivity of the magnetometer at each optical depth. The sensitivity (δB) of a magnetometer corresponds to the smallest detectable change in the magnetic field. It is given by

$$\delta B = \frac{1}{\gamma} \frac{\Delta\nu}{S/N}. \quad (1)$$

Here, the sensitivity (δB) depends on the magnetic resonance linewidth ($\Delta\nu$) measured as half-width at half-maximum (HWHM); it also depends on the S/N and on the gyromagnetic ratio (γ) of the ^{133}Cs atoms (3.5 Hz/nT).

Magnetic resonance signals are generated by slowly ramping the static magnetic field about resonance (14.285 μT) and recording the dispersive signal (Fig. 2) obtained from one of the lock-in outputs upon proper adjustment of its phase. We measure the noise in this signal to get the minimum detectable change in the magnetic field. The noise in the dispersive signal is measured with a fast-Fourier-transform spectrum analyzer when the static magnetic field is tuned on resonance. This same procedure is used in the FM BB magnetometer.

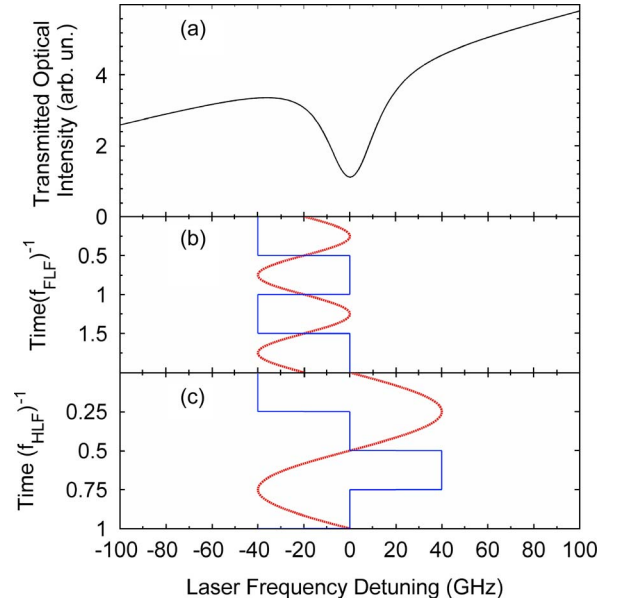


Fig. 3. (a) Absorption signal as a function of laser frequency detuning ($\Delta\nu_L$). (b) FLF modulation using sinusoidal (red dotted line) and square (blue solid line) waveforms; $f_{\text{FLF}} = f_{\text{Larmor}}$. (c) HLF modulation using sinusoidal (red) and square (blue) waveforms; $f_{\text{HLF}} = f_{\text{Larmor}}/2$.

IV. FM BB MAGNETOMETER

A. FM Waveforms

The BB magnetometer [17] differs from the Mx magnetometer in that instead of an RF field being applied, the pumping light is modulated such that it drives the coherent precession of the ^{133}Cs atoms about the external magnetic field to be measured. The pumping light frequency can be modulated by varying the VCSEL injection current at full Larmor frequency (FLF) or at half Larmor frequency (HLF). At FLF modulation, the laser frequency is centered on the side of the minimum of the pressure-broadened ^{133}Cs $D1$ transmission signal [see Fig. 3(b)]; this way, the light frequency reaches resonance once per cycle. At HLF modulation, the laser frequency is centered at the minimum of the pressure-broadened ^{133}Cs $D1$ transmission signal so that the light optical frequency reaches resonance twice per cycle [see Fig. 3(c)]. We chose to modulate the VCSEL at HLF for two reasons related with the implementation of the FM BB magnetometer in a chip-scale physics package. First, although our VCSEL was free running, in a realistic fieldable system, it could be important to lock the laser. In this situation, in the HLF scheme, it is easier to lock the laser frequency because it is centered at the minimum of the absorption signal, in contrast to the FLF modulation, where the laser frequency is centered on the side of the absorption signal. Second, in chip-scale magnetometers, the VCSEL and their leads are very close to the magnetometer sensor head, so modulation of the VCSEL injection current can cause RF magnetic fields in the sensor head. This could cause direct transitions of the atoms that alter the resonance signal on the photodiode. Therefore, it is preferable to modulate the VCSEL at a frequency different from the Larmor frequency of the atoms. For reasons described below, we investigated two types of modulation waveforms: sinusoidal and square wave. An

illustration of the different types of modulation applied for the BB excitation is shown in Fig. 3(b) and (c).

Sensitivity measurements were carried out at different atomic densities, and for each measurement, the light power was selected to yield the maximum attainable sensitivity. For low atomic densities ($OD < 0.6$), we could optimize the light power; however, for high atomic densities, due to the higher optical thickness of the atomic sample, the maximum light power available at the cell was below the optimal value and, hence, not enough to optimize the magnetometer sensitivity. We investigated the dependence of the signals on the driving modulation waveform, FM amplitude, and waveform duty cycle.

B. Sinusoidal Waveform Results

In the first attempt, we used a sinusoidal waveform to modulate the VCSEL injection current at HLF. The modulation amplitude was varied with respect to the absorption linewidth (HWHM). It was observed that the sensitivity of the BB magnetometer was lower than the sensitivity of the Mx magnetometer.

This behavior can be explained by the lower S/N of the BB magnetometer with respect to that of the Mx magnetometer. The lower S/N in the BB magnetometer is due to both a decrease in signal amplitude and an increase in noise. On the one hand, the fast passage of the VCSEL frequency through resonance decreases the time the atoms are in resonance with the pumping light. Therefore, pumping is not efficient, causing the signal amplitude to be smaller than that of the Mx magnetometer. On the other hand, the higher noise level is explained by the conversion of laser FM noise to AM noise [29]–[32] as the VCSEL frequency is scanned through the optical absorption line of the ^{133}Cs atoms. This noise conversion process can be explained by assuming that the FM noise is converted into AM noise in a linear way by the slope of the absorption profile [31]. Thus, when the light frequency is tuned to the minimum of the pressure-broadened absorption line, the noise in the signal is lower than that when the frequency is tuned on the side of the absorption line where the slope is much larger. In the Mx magnetometer, the laser frequency is not modulated but is always tuned to the minimum of the absorption line, where the FM-to-AM noise conversion is low.

For low atomic densities, we could study the effect of increasing the light power. We observed that there is an optimum light power for which the sensitivity is maximized. If we increase the light power beyond its optimum value, the signal amplitude decreases due to light broadening.

C. Square Waveform Results

To ameliorate the effects of the FM–AM noise conversion process, we modulated the VCSEL frequency with a square waveform at HLF. By changing the duty cycle (the percentage of the waveform period that the light spends on resonance) of the square waveform, we can modify the time the light spends in resonance with the atoms. Fig. 4(a) shows the signal amplitude as a function of the VCSEL frequency modulation

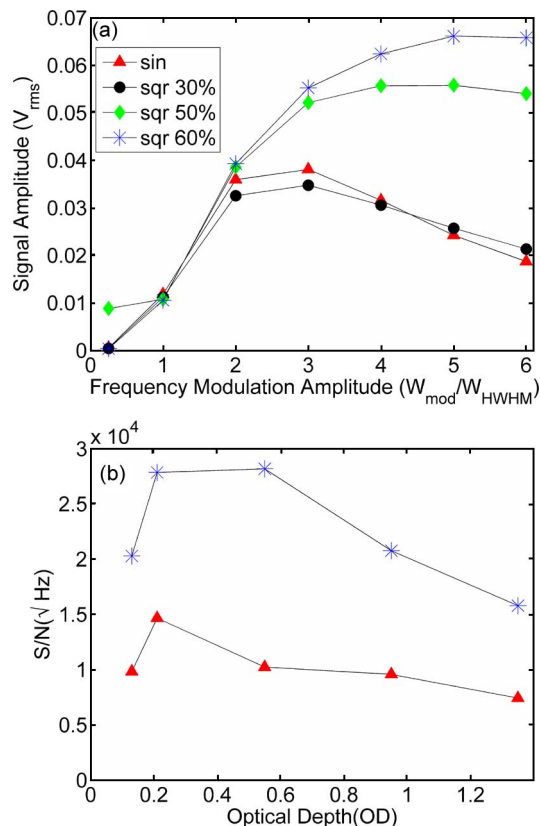


Fig. 4. (a) Signal amplitude dependence on VCSEL FM amplitude and waveform duty cycle (percentage of the waveform period that the light spends on resonance); \triangle sin—sinusoidal waveform; \circ sqr 30%—square waveform with 30% duty cycle; \diamond sqr 50%—square waveform with 50% duty cycle, $*$ sqr 60%—square waveform with 60% duty cycle. (b) Signal-to-noise ratio when the VCSEL frequency is modulated with a sinusoidal and a square waveform; \triangle —sinusoidal waveform; $*$ —square waveform with 60% duty cycle. Solid lines are used to guide the eye.

amplitude (W_{mod}). A square waveform with a duty cycle of 30% yields similar signal amplitudes as those obtained using a sine waveform. However, as the duty cycle is increased, the signal amplitude gets larger and reaches its maximum for a duty cycle of 60%. As a function of modulation amplitude (W_{mod}), the maximum signal amplitude is achieved when the modulation amplitude is about five times the linewidth (HWHM) of the pressure-broadened absorption line. This modulation amplitude represents a limit where the pumping light is modulated on and completely off resonance, enhancing the coherent precession of the atomic spin about the external magnetic field. To achieve equivalent modulation of the optical pumping rate using AM light [18]–[20], the pump would have to more or less completely be attenuated.

It is noteworthy to mention that as many as ten harmonics embedded within the square waveform are necessary to achieve the best sensitivity performance; for a larger number of harmonics, the sensitivity does not change. We verified that this was not due to the frequency-response bandwidth of the laser; our laser can respond to a higher number of harmonics embedded in the driving square waveform. For the measurements reported here, we implemented the square waveform modulation with only ten harmonics. Fig. 4(b) shows the dependence of the S/N for the sine waveform and a square waveform with 60% duty cycle.

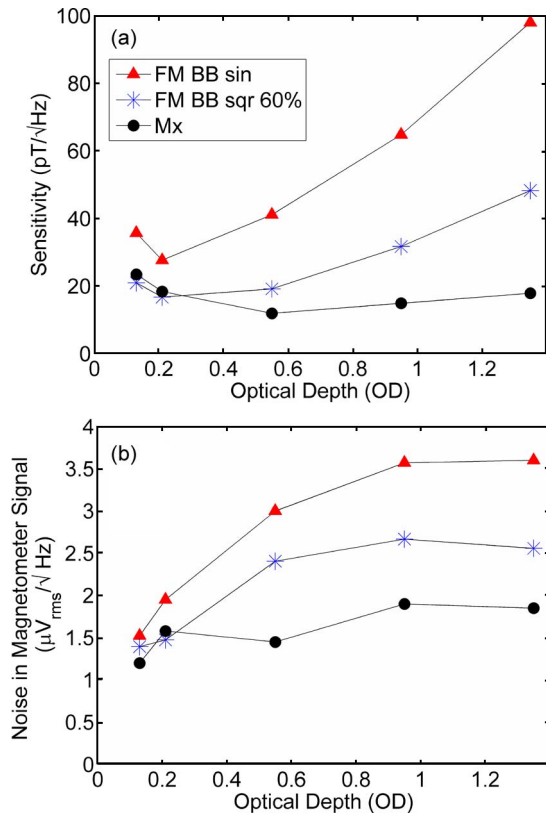


Fig. 5. (a) Magnetometer sensitivity as a function of atomic density (optical depth) for the BB magnetometer modulated with a sine waveform (Δ FM BB sin), the BB magnetometer modulated with a square waveform ($*$ FM BB sq 60%) with 60% duty cycle, and the Mx magnetometer (\circ Mx). (b) Noise in the magnetometer signal as a function of atomic density (optical depth) for the BB magnetometer modulated with a sine waveform (Δ FM BB sin), the BB magnetometer modulated with a square waveform ($*$ FM BB sq 60%) with 60% duty cycle, and the Mx magnetometer (\circ Mx). Solid lines are used to guide the eye. The light power values were optimized for the FM BB and Mx magnetometers and for each optical depth (see text).

For each of the measurements shown in Fig. 4(b), the VCSEL modulation amplitude was chosen to optimize the magnetometer sensitivity, and the light power for all measurements within each optical depth was chosen to yield the best attainable sensitivity. It is observed that the use of a square waveform yields two benefits. First, more efficient pumping is achieved, which causes the signal amplitude to be larger [Fig. 4(a)]. Second, a decrease in noise levels is realized, because the laser frequency spends less time on the slope of the absorption profile, where the noise due to the FM-to-AM noise conversion process is highest.

The sensitivity versus atomic density (optical depth) is plotted in Fig. 5(a) for the Mx magnetometer and the BB magnetometer driven by a sinusoidal waveform and a square waveform with 60% duty cycle. When the BB magnetometer is driven by a square waveform and for low atomic densities, its sensitivity is similar to that of the Mx magnetometer. For low atomic densities ($OD < 0.6$), these numbers represent the optimized sensitivities, whereas for larger atomic densities, the maximum light power was not enough to optimize the sensitivity; this and the higher noise levels in the BB magnetometer [Fig. 5(b)] could be some of the effects that cause the difference in sensitivities between the FM BB mode modulated with the

square waveform and the Mx mode at higher atomic densities ($OD > 0.6$). To improve the magnetometer sensitivity, one can increase the light power. An alternative to increasing the light power is to use a two-laser approach where one laser is dedicated to pumping and the other is dedicated to probing using phase-shift detection [3].

The best sensitivities achieved with the Mx and FM BB magnetometer correspond to 12 and 16.7 pT/√Hz, respectively, at an ambient field of 14.285 μ T. These numbers can be compared to the sensitivity of 5 pT/√Hz reached in the Mx chip-scale magnetometer [15]. The chip-scale Mx magnetometer in [15] used ^{87}Rb instead of ^{133}Cs . The difference between the gyromagnetic ratios of ^{87}Rb and ^{133}Cs , i.e., 7 and 3.5 Hz/nT, respectively, can explain the difference in sensitivities reported here and that achieved in [15].

We observe in Fig. 5(b) that the noise levels for BB and Mx magnetometers are comparable. This is explained by the use of vapor cells with high buffer gas pressure. As pointed out in [32], the effectiveness of the laser FM-to-AM noise conversion process in a vapor cell can be decreased by using buffer gas at high pressures.

V. PROSPECTS FOR THE FM BB CHIP-SCALE MAGNETOMETER

The demonstration of similar sensitivities in the Mx and FM BB magnetometer using a microfabricated vapor cell is relevant for the development of high-performance atomic magnetometers, which utilize the techniques of microelectromechanical systems. Among the advantages of microfabricated magnetometers are portability, versatility, low power consumption, and low cost of operation. Microfabricated atomic magnetometers have followed a trend toward the simplification of their design [14], [15], [33], performance improvement [15], [34], and diversification of their applications [6], [10]. The FM BB magnetometer complements all of these features.

One of the attractive features of earlier atomic magnetometers based on coherent population trapping (CPT) is that no RF magnetic fields need to be applied to the atoms to operate the instrument. However, the CPT magnetometer measures the change in the atom hyperfine energy spectrum due to the external magnetic field, and to determine the magnitude of the external magnetic field, one must subtract the nominal hyperfine splitting from the CPT magnetometer measurement. This operation makes the determination of the external magnetic field magnitude rather complex and requires the presence of a high-frequency oscillator to generate the hyperfine excitation signal. Compared to the CPT magnetometer, the BB magnetometer therefore offers simplified operation while retaining the all-optical excitation mechanism.

The FM BB magnetometer, as presented in this paper, uses electrical currents flowing near the cell outside surface to heat the vapor cell to its operating temperature. However, heating of the cell can also be achieved by the illumination of an absorbing surface with a laser; nonmagnetic temperature control of a superconducting quantum interference device (SQUID) sensor using laser absorption was described in [35]. A magnetometer based on BB excitation and optical heating would

enable a sensor without any electrical connection or metallic components close to the head sensor, thus eliminating any source of spurious magnetic fields that can affect the sensor's measurements. In addition, the all-optical FM BB magnetometer could potentially be useful in the remote detection of NMR [10], biomagnetic applications [5]–[8], and geophysical mapping.

VI. CONCLUSION

By selecting the optimum values of the operational parameters in a BB magnetometer (modulation amplitude and waveform duty cycle), we have shown that it can attain sensitivities similar to those of the M_x magnetometer. The BB magnetometer offers an advantageous solution in applications where the problems associated with the RF coils of the M_x magnetometer are not acceptable. The development of an all-optical magnetometer based on the FM BB scheme seems feasible and should enable and extend the robust application of chip-scale magnetometers.

ACKNOWLEDGMENT

The authors would like to thank D. Serkland for providing the VCSEL used in this paper and L-A Liew for providing some of the vapor cells. This paper is a contribution of the National Institute of Standards and Technology, which is an agency of the U.S. Government, and is not subject to copyright.

REFERENCES

- [1] P. Ripka, Ed., *Magnetic Sensors and Magnetometers*. Norwood, MA: Artech House, 2001.
- [2] D. Budker and M. V. Romalis, "Optical magnetometry," *Nat. Phys.*, vol. 3, pp. 227–234, Apr. 2007.
- [3] I. Kominis, T. W. Kornack, J. Allred, and M. Romalis, "A subfemtotesla multichannel atomic magnetometer," *Nature*, vol. 422, no. 6932, pp. 596–599, Apr. 2003.
- [4] J. Kitching, S. Knappe, V. Shah, P. Schwindt, W. Griffith, R. Jimenez, and J. Preusser, "Microfabricated atomic magnetometers and applications," in *Proc. IEEE Int. Freq. Control Symp.*, 2008, pp. 789–794.
- [5] G. Bison, R. Wynands, and A. Weis, "Dynamical mapping of the human cardiomagnetic field with a room-temperature, laser-optical sensor," *Opt. Exp.*, vol. 11, no. 8, pp. 904–909, Apr. 2003.
- [6] B. Lindseth, P. Schwindt, J. Kitching, D. Fischer, and V. Shusterman, "Non-contact measurement of cardiac electromagnetic field in mice using a microfabricated atomic magnetometer," in *Proc. Conf. Comput. Cardiol.*, 2007, vol. 34, pp. 443–446.
- [7] K. Kim, W.-K. Lee, I.-S. Kim, and H. S. Moon, "Atomic vector gradiometer system using cesium vapor cells for magnetocardiography: Perspective on practical application," *IEEE Trans. Instrum. Meas.*, vol. 56, no. 2, pp. 458–462, Apr. 2007.
- [8] H. Xia, A. B.-A. Baranga, D. Hoffman, and M. V. Romalis, "Magnetoencephalography with an atomic magnetometer," *Appl. Phys. Lett.*, vol. 89, no. 21, pp. 211 104-1–211 104-3, Nov. 2006.
- [9] I. M. Savukov and M. V. Romalis, "NMR detection with an atomic magnetometer," *Phys. Rev. Lett.*, vol. 94, no. 12, p. 123 001, Mar. 2005.
- [10] M. Ledbetter, I. Savukov, D. Budker, V. Shah, S. Knappe, J. Kitching, D. Michalak, S. Xu, and A. Pines, "Zero-field remote detection of NMR with a microfabricated atomic magnetometer," *Proc. Nat. Acad. Sci. U.S.A.*, vol. 105, no. 7, pp. 2286–2290, Feb. 2008.
- [11] S.-K. Lee, K. L. Sauer, S. J. Seltzer, O. Alem, and M. V. Romalis, "Subfemtotesla radio-frequency atomic magnetometer for detection of nuclear quadrupole resonance," *Appl. Phys. Lett.*, vol. 89, no. 21, pp. 214 106-1–214 106-3, Nov. 2006.
- [12] S. J. Xu, M. H. Donaldson, A. Pines, S. M. Rochester, D. Budker, and V. V. Yashchuk, "Application of atomic magnetometry in magnetic particle detection," *Appl. Phys. Lett.*, vol. 89, no. 22, pp. 224 105-1–224 105-3, Dec. 2006.
- [13] L. Langan, "A survey of high resolution geomagnetics," *Geophys. Prospect.*, vol. 14, no. 4, pp. 488–503, Dec. 1966.
- [14] P. Schwindt, S. Knappe, V. Shah, L. Hollberg, J. Kitching, L. Liew, and J. Moreland, "Chip-scale atomic magnetometers," *Appl. Phys. Lett.*, vol. 85, no. 26, pp. 6409–6411, Dec. 2004.
- [15] P. Schwindt, B. Lindseth, S. Knappe, V. Shah, J. Kitching, and L. Liew, "Chip-scale atomic magnetometer with improved sensitivity by use of the M_x technique," *Appl. Phys. Lett.*, vol. 90, no. 8, pp. 081 102-1–081 102-3, Feb. 2007.
- [16] A. Bloom, "Principles of operation of the rubidium vapor magnetometer," *Appl. Opt.*, vol. 1, no. 1, pp. 61–68, Jan. 1962.
- [17] W. Bell and A. Bloom, "Optically driven spin precession," *Phys. Rev. Lett.*, vol. 6, no. 6, pp. 280–281, Mar. 1961.
- [18] W. Gawlik, L. Krzemien, S. Pustelny, D. Sangla, J. Zachorowski, M. Graf, A. Sushkov, and D. Budker, "Nonlinear magneto-optical rotation with amplitude modulated light," *Appl. Phys. Lett.*, vol. 73, no. 13, pp. 131 108-1–131 108-3, Mar. 2006.
- [19] M. Balabas, D. Budker, J. Kitching, P. D. D. Schwindt, and J. E. Stalnaker, "Magnetometry with millimeter-scale antirelaxation-coated alkali-metal vapor cells," *J. Opt. Soc. Amer. B, Opt. Phys.*, vol. 23, no. 6, pp. 1001–1006, Jun. 2006.
- [20] S. Pustelny, A. Wojciechowski, M. Gring, M. Kotyba, J. Zachorowski, and W. Gawlik, "Magnetometry based on nonlinear magneto-optical rotation with amplitude-modulated light," *J. Appl. Phys.*, vol. 103, no. 6, pp. 063 108-1–063 108-7, Mar. 2008.
- [21] B. Chéron, H. Gilles, J. Hamel, O. Moreau, and E. Noel, "A new optical pumping scheme using a frequency modulated semi-conductor laser for ⁴He magnetometers," *Opt. Commun.*, vol. 115, no. 1/2, pp. 71–74, Mar. 1995.
- [22] H. Gilles, J. Hamel, and B. Chéron, "Laser pumped ⁴He magnetometer," *Rev. Sci. Instrum.*, vol. 72, no. 5, pp. 2253–2260, May 2001.
- [23] D. Budker, D. F. Kimball, V. V. Yashchuk, and M. Zolotarev, "Nonlinear magneto-optical rotation with frequency-modulated light," *Phys. Rev. A, Gen. Phys.*, vol. 65, no. 5B, p. 055403, May 2002.
- [24] S. J. Seltzer, P. J. Meares, and M. V. Romalis, "Synchronous optical pumping of quantum revival beats for atomic magnetometry," *Phys. Rev. A, Gen. Phys.*, vol. 75, no. 5, p. 051 407, May 2007.
- [25] S. J. Seltzer and M. V. Romalis, "Unshielded three-axis vector operation of a spin-exchange-relaxation-free atomic magnetometer," *Appl. Phys. Lett.*, vol. 85, no. 20, pp. 4804–4806, Nov. 2004.
- [26] J. Belfi, G. Bevilacqua, V. Biancalana, Y. Dancheva, and L. Moi, "All optical sensor for automated magnetometry based on coherent population trapping," *J. Opt. Soc. Amer. B, Opt. Phys.*, vol. 24, no. 7, pp. 1482–1489, Jul. 2007.
- [27] S. Groeger, A. Pazgalev, and A. Weis, "Comparison of discharge lamp and laser pumped cesium magnetometers," *Appl. Phys. B, Photophys. Laser Chem.*, vol. 80, no. 6, pp. 645–654, May 2005.
- [28] S. Knappe, V. Gerginov, P. D. D. Schwindt, V. Shah, H. G. Robinson, L. Hollberg, and J. Kitching, "Atomic vapor cells for chip-scale atomic clocks with improved long-term frequency stability," *Opt. Lett.*, vol. 30, no. 18, pp. 2351–2353, Sep. 2005.
- [29] J. C. Camparo, "Conversion of laser phase noise to amplitude noise in an optically thick vapor," *J. Opt. Soc. Amer. B, Opt. Phys.*, vol. 15, no. 3, pp. 1177–1186, Mar. 1998.
- [30] J. C. Camparo and J. G. Coffer, "Conversion of laser phase noise to amplitude noise in a resonant atomic vapor: The role of laser linewidth," *Phys. Rev. A, Gen. Phys.*, vol. 59, no. 1, pp. 728–735, Jan. 1999.
- [31] J. Kitching, N. Vukicevic, L. Hollberg, S. Knappe, R. Wynands, and W. Weidemann, "A microwave frequency reference based on VCSEL-driven dark line resonances in CS vapor," *IEEE Trans. Instrum. Meas.*, vol. 49, no. 6, pp. 1313–1317, Dec. 2000.
- [32] J. Coffer, M. Anderson, and J. Camparo, "Collisional dephasing and the reduction of laser phase-noise to amplitude-noise conversion in a resonant atomic vapor," *Phys. Rev. A, Gen. Phys.*, vol. 65, no. 3B, pp. 033807-1–033807-9, Feb. 2002.
- [33] E. Hodby, E. Donley, and J. Kitching, "Differential atomic magnetometry based on a diverging laser beam," *Appl. Phys. Lett.*, vol. 91, no. 1, pp. 011 109-1–011 109-3, Jul. 2007.
- [34] V. Shah, S. Knappe, P. Schwindt, and J. Kitching, "Subpicotesla atomic magnetometry with a microfabricated vapour cell," *Nat. Photon.*, vol. 1, pp. 649–652, Nov. 2007.
- [35] C. E. Cunningham, T. R. DeYoung, and T. A. Bouma, "Laser light heating for low-noise temperature control in SQUID applications," *Phys. B*, vol. 284–288, pp. 2111–2112, Jul. 2000.

Ricardo Jiménez-Martínez received the B.S. degree in physics engineering from Tec de Monterrey, Monterrey, Mexico, in 2004. He is currently working toward the Ph.D. degree with the Department of Physics, University of Colorado at Boulder, where he is studying atomic physics and its application to the design and construction of sensing devices.

W. Clark Griffith received the B.A. degree in physics from Whitman College, Walla Walla, WA, in 1998 and the Ph.D. degree in physics from the University of Washington, Seattle, in 2005.

Since 2007, he has been a Postdoctoral Researcher with the Time and Frequency Division, National Institute of Standards and Technology, Boulder, CO, working on developing MEMS-based alkali atom magnetic sensors.

Ying-Ju Wang received the B.S. degree in physics and the M.S. degree in electro-optical engineering from the National Taiwan University, Taipei, Taiwan, in 1996 and 1998, respectively, and the Ph.D. degree in physics from the University of Colorado at Boulder in 2005.

From 2005 to 2008, she was a Postdoctoral Associate with the Optical Frequency Measurements Group, Time and Frequency Division, National Institute of Standards and Technology, University of Colorado at Boulder. She is currently a Senior Scientist with Cymer, Inc., San Diego, CA. Her research experiences include integrated optical devices, laser spectroscopy, chip-scaled atomic devices such as atom interferometers and atomic magnetometers, and advanced light source.

Svenja Knappe received the Diploma in physics, with a thesis topic on the investigation of single cesium atoms in a magneto-optical trap, and the Ph.D. degree, with a thesis on "Dark resonance magnetometers and atomic clocks," from the University of Bonn, Bonn, Germany, in 1998 and 2001, respectively.

Since 2001, she has been with the Time and Frequency Division, National Institute of Standards and Technology, Boulder, CO. Her research interests include the miniaturization of atomic sensors, precision laser spectroscopy, atomic clocks and magnetometers, laser cooling, alkali vapor cell technology, applications of semiconductor lasers to problems in atomic physics, and frequency control.

John Kitching received the B.Sc. degree in physics from McGill University, Montreal, QC, Canada, in 1990 and the M.Sc. and Ph.D. degrees in applied physics from the California Institute of Technology, Pasadena, in 1995.

He is currently a Physicist with the Time and Frequency Division, National Institute of Standards and Technology, Boulder, CO. His research interests include atomic frequency standards, low-noise microwave oscillators, atomic magnetometers, and gyroscopes.

Ken Smith was born in Toronto, ON, Canada. In 1975, he joined Geometrics, Canada, on a part-time basis while continuing his studies.

He is currently an Engineer with Geometrics, Inc., San Jose, CA, where he has worked on the design of all of the current magnetometers and was the Lead Engineer on all of the cesium-based magnetometers. He is the holder of several important patents in this area.

Mark D. Prouty (M'84) received the B.A. degree in physics from the University of Chicago, Chicago, IL, in 1978 and the M.S. and Ph.D. degrees in electrical engineering from the University of California, Berkeley, in 1984 and 1994, respectively.

He has been the President of Geometrics, Inc., San Jose, CA, since 1999. Geometrics, Inc., is a world leader in the design, manufacture, and support of geophysical instruments, including near-surface exploration seismographs, magnetometers for exploration and unexploded ordnance (UXO) detection, and electromagnetic systems for exploration. His research interests include low-power atomic magnetometers and most other technologies for geophysical exploration.